Astron. Astrophys. 67, 409—420 (1978)

ASTRONOMY
AND
ASTROPHYSICS

Old Supernova Remnants as Magnetohydrodynamic Wave Fronts

Formation of Filamentary Structure

Y. Sofue*
Max-Planck-Institut für Radioastronomie, Auf dem Hügel 69, D-5300 Bonn, Federal Republic of Germany

Received October 12, 1977

Summary. Expanding shells of old supernova remnants (SNR) are simulated by magnetohydrodynamic (MHD) wave fronts. We examine the three-dimensional behavior of the shells interacting with the inhomogeneous interstellar medium and clouds. The wave front undergoes strong refraction and reflection by the clouds. Subsequent focusing of the waves produces filamentary structures and bright patches, when the cloud size is much smaller than the shell radius. If the cloud size is comparable with or greater than the shell radius, the SNR becomes greatly deformed from a sphere. Morphological features of a typical old SNR, S 147, are fit reasonably well by a model which postulates interaction with several interstellar clouds of radii 8–12 pc.

Key words: supernova remnant — magnetohydrodynamic waves — interstellar clouds

1. Introduction

Old supernova remnants (SNR) are characterized by their shell structures. The shells are observed to deviate from a circular shape and to have a complicated morphology composed of many arc filaments. This suggests strong interactions of the shells with an inhomogeneous interstellar medium.

Formation of the shell structure in an advanced stage of SNR has been investigated theoretically by a number of authors using hydrodynamic codes to follow shock waves through the interstellar gas (e.g., Cox, 1972a, b; Chevalier, 1974; Straka, 1974). In these works the SNRs are treated as one-dimensional spherical shocks expanding into a homogeneous medium. To study further structure such as filaments and non-spherical shapes, two-dimensional models have been proposed: Sgro (1975) and McKee and Cowie (1975) have calculated the interactions of the shock waves with dense clouds; Chevalier and Gardner (1974) have examined the effect of the plane-stratified structure of the galactic disk on an SNR of extremely large-radius. However, the existing models seem too simple to reproduce the highly structured features such as arc filaments in the observed SNRs, which must require an understanding of the three-dimensional case.

In the present paper, we discuss the advanced stage of SNRs characterized by the shell structures with special reference to the influence of interstellar clouds. The expanding SNR shell is approximated by a magnetohydrodynamic (MHD) wave front. We follow its three-dimensional behavior as it propagates through an inhomogeneous interstellar medium with magnetic fields. We propose a mechanism of formation of arc filaments and bright patches in old SNRs through refraction and focusing of the MHD waves by the interstellar clouds. The result is used to get information about locations, sizes, densities and magnetic fields in the interstellar clouds by a comparison with a typical old SNR, S 147.

2. MHD Waves in Interstellar Space

A method to trace the fast-mode MHD waves in a magnetized plasma in the solar corona has been developed by Uchida (1970, 1974) and Uchida et al. (1973). This method has been applied to a galactic-scale phenomenon associated with activity in the galactic center (Sofue, 1976a, 1977). In the present paper, we apply the method to old SNR shells expanding into the interstellar medium.

The propagation of the fast-mode MHD wave is independent of magnetic field configuration, and depends only on the distribution of the magnitude of Alfven velocity (Uchida, 1970). This approximation is valid when the square of Alfven velocity, V^2, is much greater than that of sound velocity, c_s^2, namely, $(V/c_s)^2 \gg 1$. We summarize in Table 1 the physical quantities in the interstellar medium. From this table, we see that the ratio (V^2/c_s^2) is sufficiently large compared with unity: ~ 10 for intercloud gas, and ~ 200 for typical interstellar clouds. It is therefore reasonable to apply Uchida's

* Senior Humboldt Fellow on leave from Department of Physics, Nagoya University, Nagoya, Japan

Table 1. Physical quantities in the Interstellar Medium

Quantities	Intercloud gas	Standard H I-cloud	H I-cloud which has contracted from intercloud medium with "frozen-in" field
Density, n (cm^{-3})[a,b]	0.05–0.1	10	10
Magnetic fields, B (Gauss)[b]	$4\,10^{-6}$	$20\,10^{-6}$	$90-140\,10^{-6}$
Alfven velocity, V (km s^{-1})	30–40	14	60–100
Sound velocity, c_s (km s^{-1})	11	1	1
V^2/c_s^2	7–14	200	$0.4-1\,10^4$

Values for intercloud gas and standard H I-clouds are from:
[a] Spitzer (1968) and
[b] Heiles (1976)

method to the behavior of fast-mode MHD waves in interstellar space.

The equations describing the propagation of a MHD wave packet of small amplitude are written as follows (Uchida, 1970):

$$\frac{dr}{dt} = V p_r/p, \tag{1}$$

$$\frac{d\theta}{dt} = V p_\theta/rp, \tag{2}$$

$$\frac{d\phi}{dt} = V p_\phi/rp \sin\theta, \tag{3}$$

$$\frac{dp_r}{dt} = -p\frac{\partial V}{\partial r} + \frac{V}{rp}(p_\theta^2 + p_\phi^2), \tag{4}$$

$$\frac{dp_\theta}{dt} = -\frac{p}{r}\frac{\partial V}{\partial \theta} - \frac{V}{rp}(p_\theta p_r - p_\phi^2 \cot\theta), \tag{5}$$

$$\frac{dp_\phi}{dt} = -\frac{p}{\sin\theta}\frac{\partial V}{\partial \phi} - \frac{V}{rp}(p_\phi p_r + p_\phi p_\theta \cot\theta), \tag{6}$$

where $V = V(r,\theta,\phi) = V(x,y,z)$ is the Alfven velocity, the vector $\boldsymbol{p} = (p_r, p_\theta, p_\phi)$ is defined through a phase function, or an eikonal, Φ, as $\boldsymbol{p} = \text{grad}\ \Phi$ with $p = (p_r^2 + p_\theta^2 + p_\phi^2)^{1/2}$, and (r,θ,ϕ), (x,y,z) are the spherical and cartesian coordinates of the position of a wave packet, respectively. Once the distribution of the Alfven velocity V is given, we can trace the three-dimensional propagation of the MHD waves by integrating Equations (1)–(6).

The dissipation rate γ for MHD waves is given by

$$\gamma = \frac{\omega}{2V^3}\left(\frac{\eta}{\rho} + \frac{c^2}{4\pi\sigma_e}\right) \tag{7}$$

(Landau and Lifshits, 1960), where γ is defined through the relation, amplitude $\propto \exp(-\gamma l)$. Here ω is the frequency of the wave, η the viscosity, σ_e the electric conductivity, c the light velocity, ρ the gas density, and l is the distance along the ray path. In interstellar space, the second term is negligible compared with the first. If we adopt the molecular viscosity for η and assume that $V = 40\,\text{km s}^{-1}$, $\omega = 2V/\Delta l$ and $\Delta l = 2$ pc as the typical thickness of the filaments, then we have $1/\gamma \approx 800$ pc. This value is large enough compared with the radius ~ 30 pc of old SNRs considered here. Hence, we may neglect the dissipation of the waves in the present circumstances.

3. MHD Wave Front Interacting with Interstellar Clouds

A simple computation of a spherical shock wave to simulate a SNR by Cox (1972a) shows that the expansion velocity of SNR at a radius $r \gtrsim 30$ pc decreases to 50 km s^{-1} or less, which is comparable with the Alfven velocity in the intercloud medium (Table 1). Supernova remnants like S 147 may be in this stage, which corresponds to the Stages III and IV in Woltjer's (1972) terminology. A neutral hydrogen observation of HB 21, which may be similar to S 147, shows an expansion velocity of about 25 km s^{-1} (Assousa and Erkes, 1973). This velocity is supersonic, but sub-Alfvenic. We may therefore assume that the expansion velocity of the shell in the late stage ($t \gtrsim 5\,10^5$ yr) of Type-II SNR of normal energy is comparable with the local Alfven velocity.

The SNR shock front in this stage will excite the fast-mode MHD waves, whose propagation velocity is the highest of all modes in interstellar space. We assume here that the kinetic energy of the shell is converted into a MHD blast waves of fast-mode at $r \gtrsim 20$–30 pc; namely, we approximate the SNR shell by the MHD blast wave. By this approximation, we can follow the three-dimensional behavior of the expanding shell through the inhomogeneous medium.

We assume the following form for the spatial distribution of Alfven velocity:

$$V = V_0\left\{1 + \sum_i \varepsilon_i \exp\left[-\frac{(x-x_i)^2}{\sigma_{x_i}^2} - \frac{(y-y_i)^2}{\sigma_{y_i}^2} - \frac{(z-z_i)^2}{\sigma_{z_i}^2}\right]\right\}. \tag{8}$$

Here the position of the i-th cloud is denoted by (x_i, y_i, z_i) and its extent in the x, y and z directions by $(\sigma_{x_i}, \sigma_{y_i}, \sigma_{z_i})$. Enhancement of Alfven velocity in the cloud is represented by ε_i: if $\varepsilon_i \gtrsim 0$, the velocity increases toward the cloud center and the cloud is regarded as a

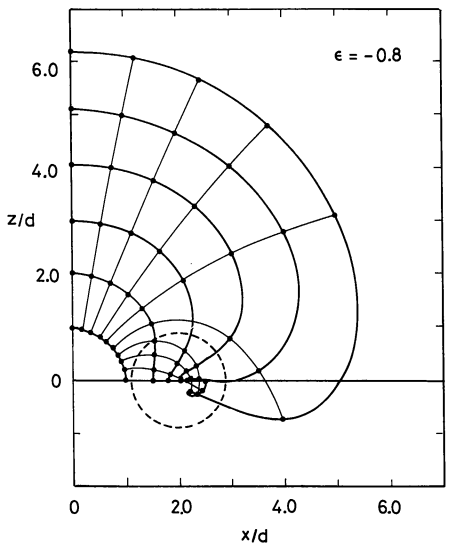

Fig. 1. Propagation of magnetohydrodynamic waves in the presence of a low-V cloud ($\varepsilon=-0.8$) located at $x=2d$ with the size $\sigma=1d$. Thick lines are wave fronts, and thin lines are wave paths. Here d denotes the scaling factor with a dimension of length. The waves are refracted by the cloud and a focusing occurs similar to that of a convex lens in optics

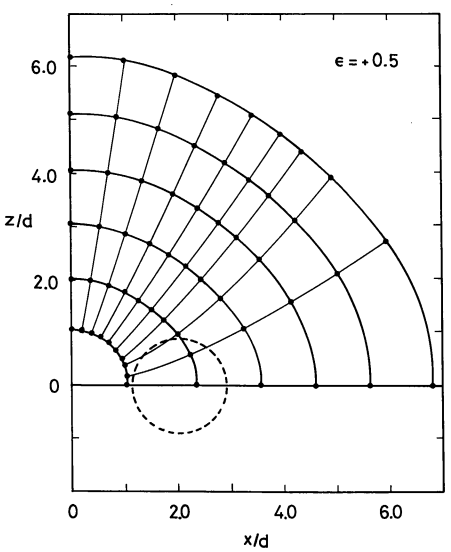

Fig. 2a. The same as Figure 1 but for a high-V cloud of $\varepsilon=0.5$. The waves diverge on encountering the cloud

magnetic "wall" or a barrier (Uchida, 1975), where the waves are reflected outwards. If $\varepsilon_i<0$, the cloud is a magnetic "valley" or a sink, into which the waves focus.

We now integrate Equations (1)–(6) for this Alfven velocity distribution. As an initial condition at $t=0$ of computation, we distribute MHD wave packets on a small sphere centered at $(x, y, z)=(0, 0, 0)$. Each wave packet is initially given a constant radial velocity.

To see the typical behavior of the MHD waves, we give some simple examples.

i) A Spherical Cloud with Low Alfven Velocity

We first examine the case of the front encountering a spherical cloud with $\varepsilon=-0.8$ and $(\sigma_x, \sigma_z)=(d, d)$ located at $(x, z)=(2d, 0)$, where d denotes a normalized distance with a dimension of length. At the center of the cloud, the Alfven velocity decreases to 20 percent of that in the surrounding region: $V=(1+\varepsilon)V_0$. Figure 1 shows the propagation of wave packets in the (x, z) plane which includes the cloud center. The time interval between the fronts in this figure is $\Delta t=d/V_0$: if $d=5$ pc and $V_0=40$ km s^{-1}, we have $\Delta t=1.25\,10^5$ yr.

When the front encounters a cloud, the ray paths are refracted toward its center and the propagation is decelerated. The front forms a concave surface, and finally the refracted rays focus into a small region in the cloud slightly away from the center: The cloud therefore plays a role similar to a convex optical lens. Such focusing may produce a bright knot in or behind the cloud (see the next section).

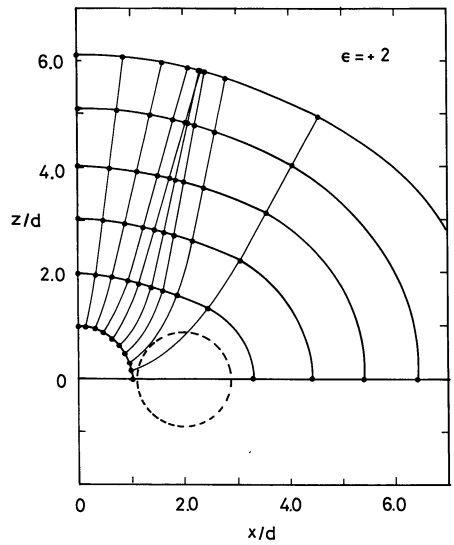

Fig. 2b. The same as Figure 2a, but for a higher-V cloud ($\varepsilon=2$). Strongly reflected rays converge to a point at $(x, z)\simeq(2d, 5d)$, producing a string-like filament as is shown in Figure 7. Note that the cloud behaves as a "barrier"

ii) A Spherical Cloud with High Alfven Velocity

Figures 2a and b show the results when the front encounters clouds of enhanced Alfven velocity, $\varepsilon=0.5$ and 2, respectively, with $(\sigma_x, \sigma_z)=(d, d)$ and $(x, z)=(2d,0)$. In this case, the cloud is similar to a concave lens. The rays diverge on passage through the cloud, forming a protuberance toward the cloud. As the shell expands further, a portion of the refracted rays converge into a small region as shown in Figure 2b (at $x\approx 2d$, $z\approx 5d$), provided the value of ε is large enough. As shown in Section 4, this focusing effect may produce a ring-shaped

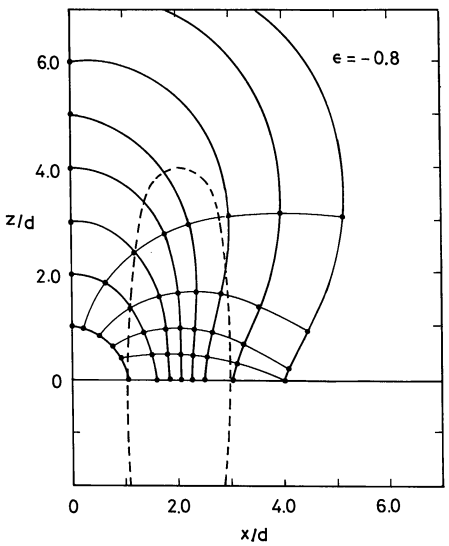

Fig. 3. Propagation of MHD waves encountering an elongated cloud of low Alfven velocity ($\varepsilon = -0.8$)

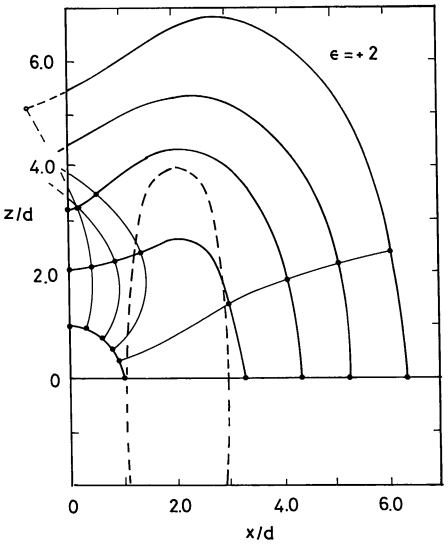

Fig. 4. Propagation of MHD waves encountering an elongated cloud of high Alven velocity ($\varepsilon = 2$)

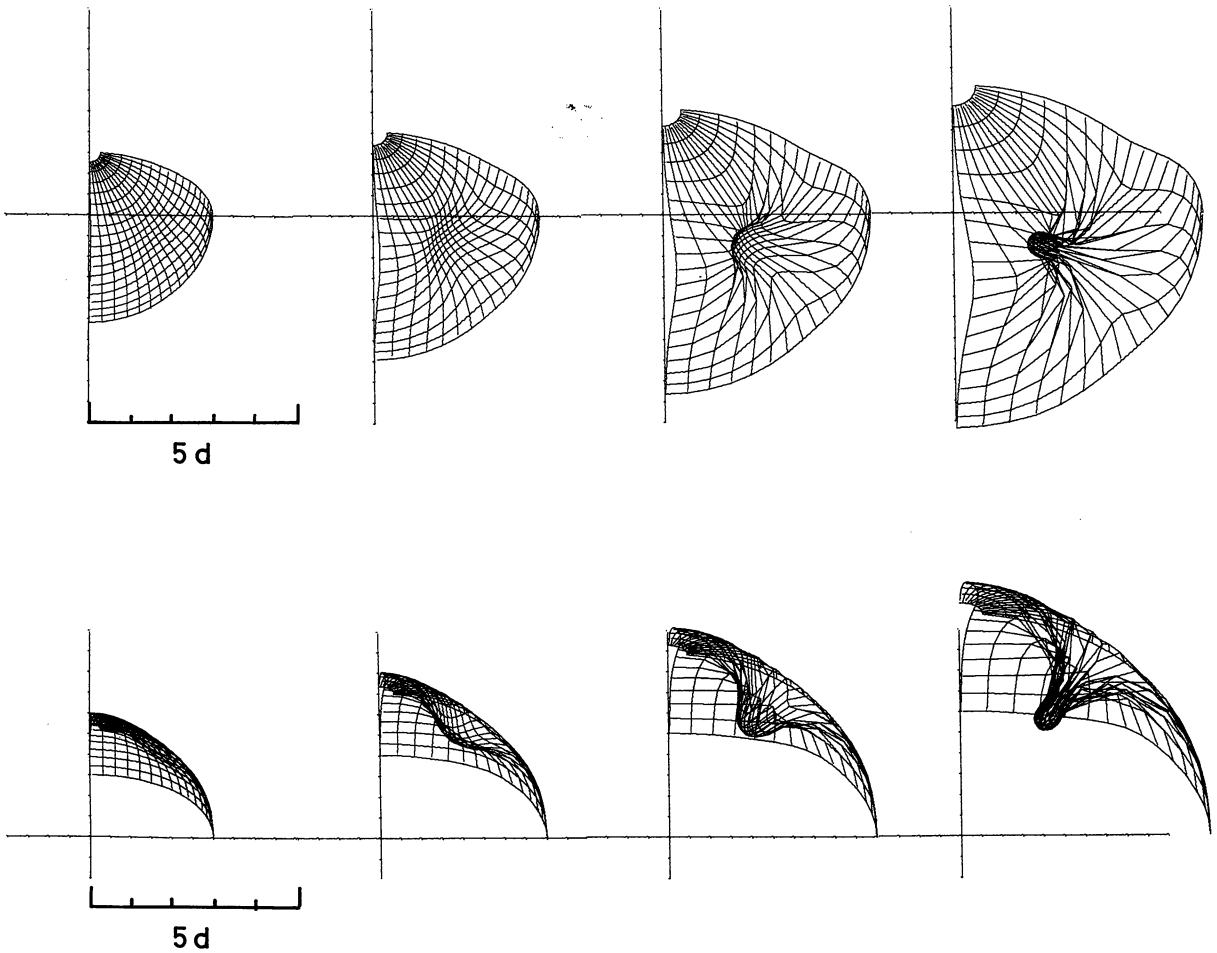

Fig. 5. MHD wave front encountering a spherical, low-V cloud ($\varepsilon = -0.95$) located at $(x, y, z) = (2d, 2d, 2d)$ and $\sigma = 1d$. The upper diagrams show the views from a line of sight at an angle of 60° to the $x-y$ plane; the lower diagrams show edge-on views. The time interval is $\tau = d/V_0$. A filamentary structure is simulated by a projection of a corrugated surface which has been focused by the cloud (second and third diagrams). As the front expands further, a bright patch appears with a high wave density (last diagram)

filament, or a string of high energy density, around the cloud.

iii) Elongated Clouds

If the cloud is elongated in the x-direction and $\varepsilon<0$, the behavior of the rays is essentially the same as in Case i). The rays focus into a small region near the major axis, producing a bright knot. If $\varepsilon>0$, the rays strongly diverge outwards, but no significant focusing takes place. The deformation of the shell is stronger than in Case ii).

Figure 3 shows the front encountering a cloud elongated in the z-direction with $\varepsilon=-0.8$, $(\sigma_x, \sigma_z)=(1d, 4d)$ at $(x, z)=(2d,0)$. In this case, the focusing in the (x, z)-plane takes place after the rays penetrate the cloud. If $\sigma_y=\sigma_x$, the behavior in the (x, y)-plane is the same as in Case i). The elongated cloud is therefore similar to a cylindrical lens. Figure 4 gives the result for a cloud of $\varepsilon=2$ with the same shape as above. The rays are more strongly reflected outward than in the case of spherical clouds and the shell is greatly deformed.

4. Formation of Filamentary Structures and Bright Knots

In this section, we follow the three-dimensional behavior of the MHD wave fronts, and display the results as mesh surfaces, each mesh point of which represents the position of a wave packet.

i) Filaments of Thin Sheets Seen Edge-on

As shown in Figure 1, the MHD front is corrugated to form a concave surface, when it encounters a cloud with a low Alfven velocity. In this concave front, the energy flux of the MHD waves is higher than in the surrounding regions. Figure 5 shows the MHD front as a mesh surface. The front encounters a cloud of low Alfven velocity: $\varepsilon=-0.95, (\sigma_x, \sigma_y, \sigma_z)=(d, d, d)$, located at $(x, y, z)=(2d, 2d, 2d)$. When this concave part is looked at face-on, we may observe only an enhancement of brightness in the cloud, as is the case in the earlier stage in Figure 5 (upper part). However, if this focusing takes place near the limb of the SNR, we can observe a sharp filamentary structure as a result of an edge-on view of the corrugated front [Fig. 5 (lower part)].

This sort of filament, which is not a true filament, but rather a projection effect of the corrugated sheet, is characterized by the fact that its center of curvature is on the outward side of the sheet, that is, away from the center of the SNR. A long, strong filament near the southern limb of S 147 may be a typical example of this edge-on sheet filament (see Section 6).

ii) Bright Knots

If the Alfven velocity in a cloud is much smaller than that of the surrounding region, the rays strongly focus on the central region of the cloud. As shown in the later stage in Figure 5, the MHD waves form there a deeply concave front of high energy flux density. The focal region illuminated by the refracted rays will appear as a bright knot. In the NE quadrant of S 147, we can observe such a bright region. As shown in Section 6, the cloud responsible for this knot should have a radius of 8 pc.

The convergence will result in an increase of the shock strength, similar to an implosion of a spherical shock toward the center. The strong shock may cause some interesting phenomena such as a fragmentation of the cloud and star formation (see Section 7 ii).

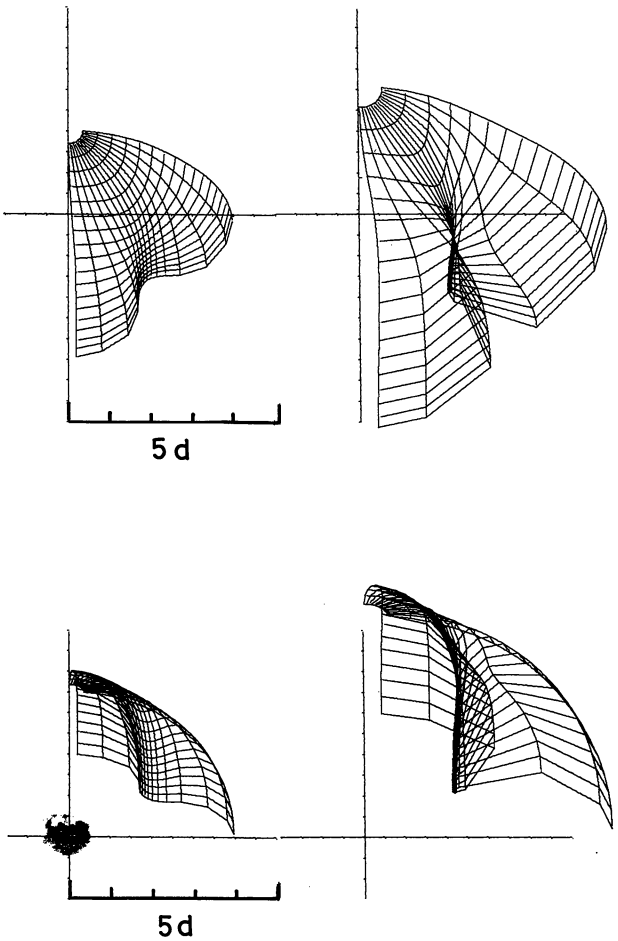

Fig. 6. The same as Figure 5, except that the cloud is elongated in the z-direction; $(\sigma_x, \sigma_y, \sigma_z)=(1d, 1d, 5d)$. The rays focusing along the axis of the cloud form a filamentary structure extending in the z-direction

iii) Long, Straight Filaments

Figure 6 shows a front encountering a low-V cloud elongated in the z-direction, $\varepsilon=-0.8$, $(\sigma_x, \sigma_y, \sigma_z)=(d, d, 5d)$, and located at $(x,y,z)=(2d,2d,d)$. In this case, a long string of focusing waves appears along the major axis of the cloud. The Cygnus Loop has a long, wavy filament across the central region, which might be

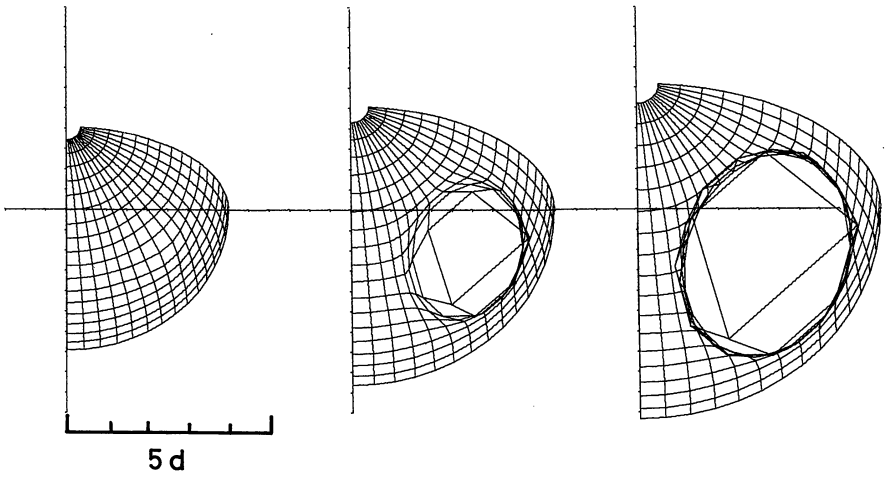

Fig. 7. MHD wave front encountering a high-V spherical cloud of $\varepsilon=2$ and $\sigma=1d$ located at $(x,y,z)=(2d,2d,2d)$. The reflected rays focus into a thin string, or a circular filament thereby creating a hole on the front surface

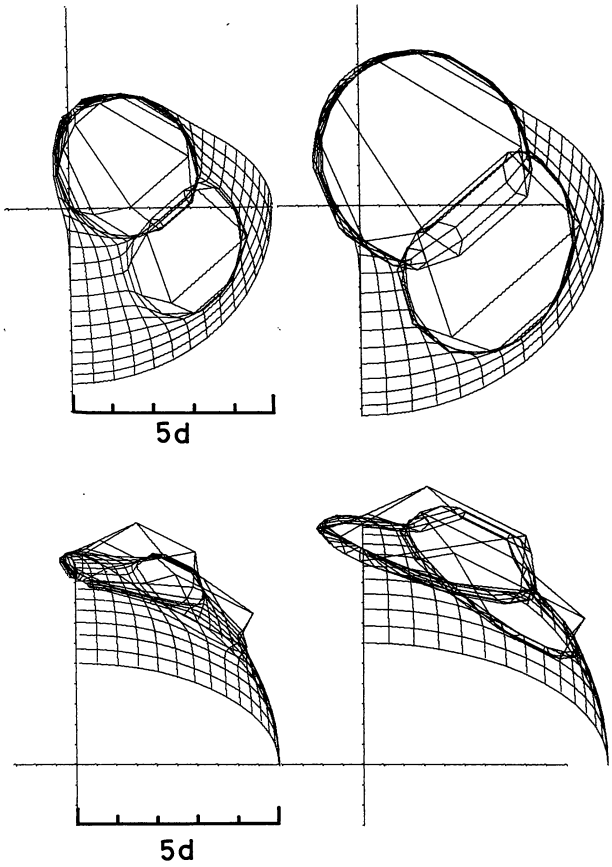

Fig. 8. The same as Figure 7, but there are two high-V clouds of the same scale. Some complicated filamentary structures appear as the result of a projection effect

understood in the present model. However, we must keep in mind that the Cygnus Loop is in a rather younger stage than old SNRs such as S 147, and the present approximation should be regarded as giving only the qualitative behavior. A non-linear shock treatment of the three-dimensional case is necessary for a more accurate discussion.

iv) Arc-string Filaments

When the MHD front encounters a high-V cloud, the rays are reflected outward and converge into a thin ring (Fig. 2b). Figure 7 shows the behavior of a front against a cloud of $\varepsilon=2$, $(\sigma_x, \sigma_y, \sigma_z)=(d, d, d)$ at $(x, y, z)=(2d, 2d, 2d)$. The rays are reflected near the surface of cloud, and converge to produce a thin and sharp focal ring of high energy flux density around the cloud, which will be observed as an arc filament. This type of filament is a "true" filament, or a string, and should be distinguished from the edge-on filament which is the result of the projection effect discussed in Section i). This sort of string is not necessarily associated with the outer limb, but can appear anywhere on the SNR shell. A typical example may be the sharp and thin arc in the southern quadrant of S 147, near its center (filament *f* in Fig. 14b). The orientation of this arc seems to be independent of the outer filamentary shell, and also of the whole shell structure.

If two or more clouds of high V are located close to each other, some interesting features may appear: Figure 8 gives the result with two clouds of the same radius, $(\sigma_x, \sigma_y, \sigma_z)=(d, d, d)$ and $\varepsilon=2$. They are located at $(1.5d, 1.5d, 4.7d)$ and $(3d, 3d, 3d)$, namely, they are at the same distance $r=5.2d$ from the SNR center and separated $2.7d$ from each other. The formation of a ring filament around each cloud is essentially the same as in Figure 7. However, a filament produced by the first cloud suffers again from a strong refraction by the other, and its refracted part disappears. As a consequence, two arc filaments appear, contacting each other at some angle. We can often recognize such filaments, which are sharply bent in their middle, in old SNRs.

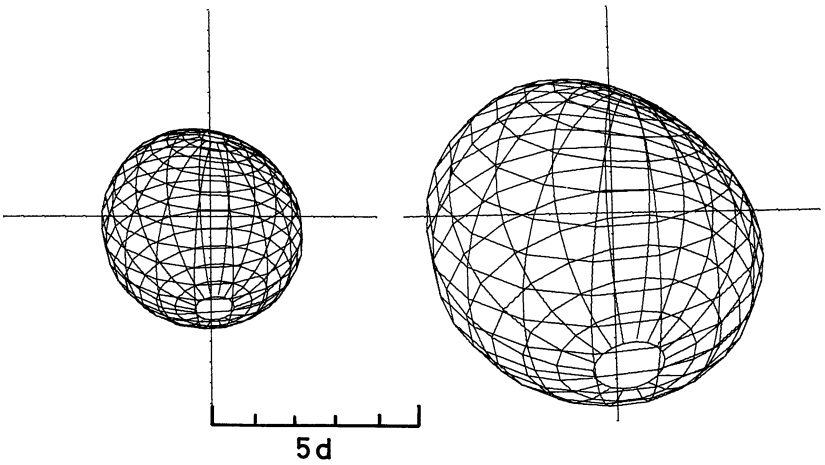

Fig. 9. MHD wave front encountering a large scale, low-V cloud ($\varepsilon=-0.8$) located at $(x,y,z)=(3d,3d,3d)$ with $\sigma=5d$. The waves penetrating the clouds are decelerated and the shell deforms from a sphere

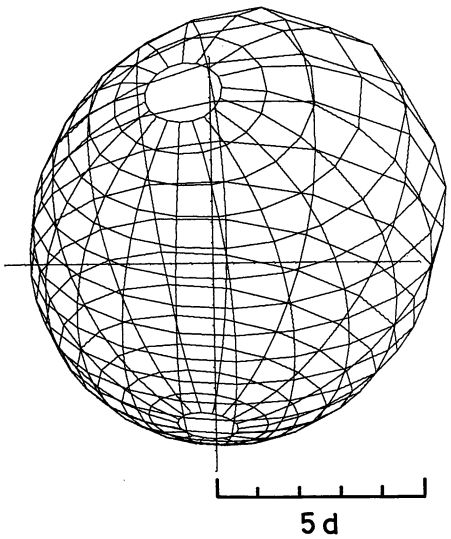

Fig. 10. The same as Figure 9 but for a high-V cloud ($\varepsilon=1$). A protuberance appears where the wave density is lower and the spherical such as CTB 1 and IC 443

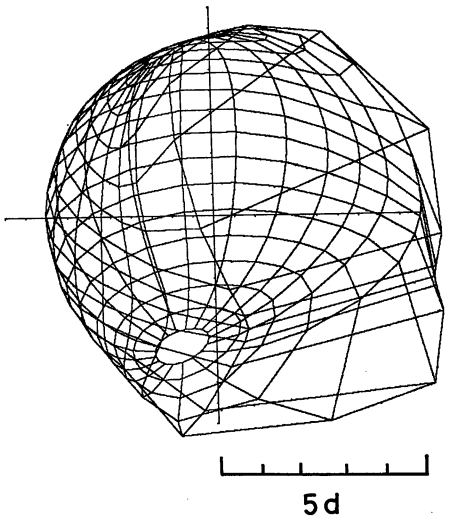

Fig. 11. An expanding MHD shell encountering two large clouds of high Alfven velocity ($\varepsilon=1$); $(x, y, z)=(2d, 2d, 2d)$ and $(2d, 2d, -2d)$ respectively with $\sigma=2d$. Strong deformation from a sphere occurs, resulting in an asymmetric shell, which resembles some old SNRs such as CTB 1 and IC 443

5. Large-scale Deformation of a SNR Shell

In addition to the filaments and bright knots, old SNRs usually show a large-scale deformation from a circular shell structure. This may be easily understood as a result of the interaction of the shell with large-scale irregularities of characteristic sizes comparable with the SNR radius or larger. To examine the influence of such large-scale inhomogeneities, we calculated the following two cases: i) the MHD waves encounter large-scale clouds; ii) the MHD front expands into a plane-stratified medium. The latter presumes the influence of the galactic gaseous disk on very large SNR shells whose radius is comparable with or larger than the scale thickness ($\sim$100 pc) of the disk: $r \gtrsim 50$ pc.

i) Large Clouds

When the MHD shell encounters a low-V cloud of large radius, a considerable part of the front facing the cloud is decelerated, and the whole shell greatly deforms from a spherical shape. Figure 9 shows an example for the case of $(\sigma_x, \sigma_y, \sigma_z)=(5d, 5d, 5d)$, $(x, y, z)=(3d, 3d, 3d)$ with $\varepsilon=-0.8$. Such features appear in some old SNRs such as HB 9 and OA 184 (see, e.g., van den Bergh et al., 1973).

If the encounter is with a high-V cloud, a large part of the shell expands with higher velocity into the cloud, forming a protuberance. Figure 10 gives a result for the case of $\varepsilon=1$ with the other parameters the same as in Figure 9. Such a protuberance may explain the large-

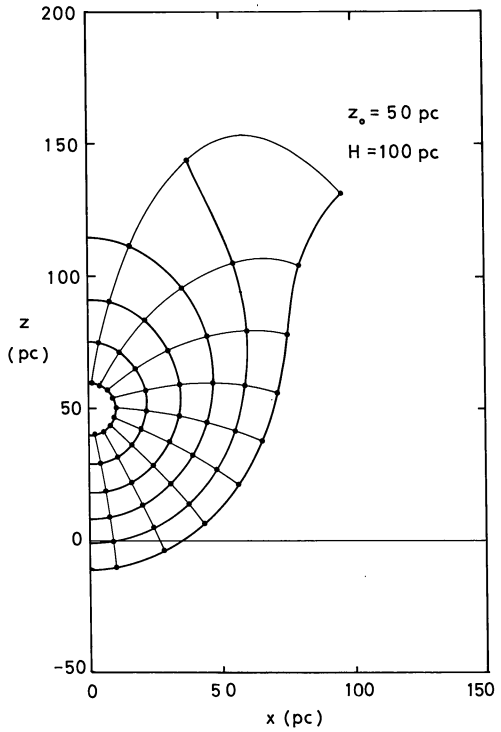

Fig. 12a. Propagation of MHD waves in a plane-stratified medium where the Alfven velocity varies as a function of z as $V=V_0 \exp(z^2/H^2)$ with $H=100$ pc. The waves are radiated isotropically at $z=z_0=50$ pc. This figure simulates the evolution of the remnant of a supernova which exploded at a height of $z_0=50$ pc above the galactic plane. The shell deforms from a sphere when the radius exceeds ~ 50 pc

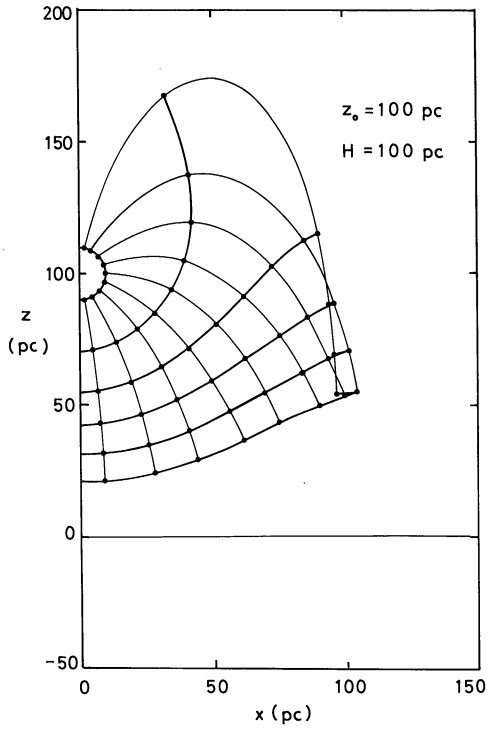

Fig. 12b. The same as Figure 12a, except that the explosion occurs at higher z ($z_0=100$ pc above the galactic plane). The shell dissipates after its radius exceeds ~ 40 pc

scale deformation observed in the southern region in the Cygnus Loop.

Figure 11 shows the case of two clouds with $\varepsilon=1$ and radius$=2d$, located at $(x, y, z)=(2d, 2d, 2d)$ and $(2d, 2d, -2d)$ respectively. The shell is so strongly deformed that the half of the shell facing the clouds practically disappears. As a consequence, an incomplete arc structure remains on the opposite side of the clouds. We suggest that VRO 420501, RCW 86 and CTB 1 may be typical examples of SNRs which have been deformed in such a manner.

A large-scale deformation of the south-western part of IC 443 may be also explained in this manner. It is interesting to note that a bright north-eastern shell of this SNR has been shown to interact with a dense CO cloud with extent of 2–4 radii of the SNR (Cornett et al., 1977).

ii) Plane-stratified Disk

The gaseous disk of our Galaxy has a scale thickness of 50–100 pc ($=h_g$). On the other hand, the radio background emission shows that the non-thermal radio disk, which is composed of magnetic fields and cosmic-ray electrons, has a half thickness of 500 pc (e.g., Sofue, 1976b); namely, the magnetic disk has a half thickness of about $h_m=500$ pc. If we assume that the gas density and magnetic pressure are distributed plane parallel in the form of $\exp(-z^2/h_g^2)$ and $\exp(-z^2/h_m^2)$, respectively, the Alfven velocity is expressed as

$$V=V_0 \exp(Z^2/H^2), \tag{9}$$

where $H=\sqrt{2}\, h_g h_m/(h_m^2-h_g^2)^{1/2} \simeq \sqrt{2}\, h_g$ since $h_g^2 \ll h_m^2$.

We now examine the behavior of the MHD front in the plane-stratified disk of a scale thickness H. Of course, the galactic effect is not very significant if the radius of the SNR is small compared with H, or $r \lesssim 40$ pc. However, if $r \gtrsim 50$ pc, the effect becomes important. In Figure 12, we show the behavior of the ray paths and fronts in the $(x-z)$ plane for the cases that the SNR explosion takes place at heights of $z_0=50$ pc and 100 pc above the galactic plane. Here we assumed that $H=100$ pc. In the initial stage of the expansion, the shell remains spherical. If the radius exceeds ~ 50 pc, however, the front will be strongly affected by the z-variations of the Alfven velocity: the upper part of the shell will open suddenly to form a dish-like surface. This shape is the result of the reflection of the waves, caused by the steep increase of V toward the high-z region.

From this calculation, we see that a SNR can hardly retain a spherical shell and is almost completely broken up if its radius exceeds ~ 50 pc. In this context, it is of

Table 2. Parameters for clouds around S 147

No. of cloud	Position (pc)[a]			Size (pc)			ε	Alfven velocity (km s^{-1}) at the cloud center $V_0(1+\varepsilon)$		Corresponding feature in Fig. 14b
	x	y	z	σ_x	σ_y	σ_z		$V_0=30$	40 km s^{-1}	
1	− 4	−16	−16	20	8	8	−0.9	3	4	a
2	−12	12	12	8	8	8	−0.95	1.5	2	b
3	−24	0	− 4	10	10	10	1	60	80	c
4	24	0	8	12	12	12	2	90	120	d
5	− 8	8	24	8	8	8	0.6	50	64	e

[a] Position is referred to the center of the SNR. The coordinate system and the spatial relation of the clouds are illustrated in Fig. 13

interest to note that some galactic spurs, the so-called Loops I–IV, of radio continuum have been suggested to be very old SNRs with radii ~100 pc or more. However, we must conclude that it is quite difficult for SNR shells to remain in a loop structure in such an extremely late stage.

6. Application to the Supernova Remnant S 147

Our computations so far have been for the cases that the MHD front encounters one or two simple clouds. However, interstellar space must be occupied by many clouds of different parameters. If we combine several clouds of high and low Alfven velocities, we may be able to reproduce more complicated structures in actual SNRs. Furthermore, model fitting of the computed result to the observed SNR morphology should make it possible to obtain information about the physical parameters of the clouds.

As an example, we now discuss the SNR, S 147. S 147 is a typical old SNR, well known for its beautiful shape which is rich in long and delicate filaments. Its radius is estimated to be ~35 pc. (Downes, 1971). This SNR is therefore in the evolutionary Stages III andIV of Woltjer's (1972) terminology which van den Bergh et al. (1973) call "the S 147 type". The Vela nebulosity is also classified in this type. Irregular filamentary nebulosities in the Vela SNR (e.g., Elliott et al., 1976), which indicate the strong influence of a highly inhomogeneous interstellar medium, might also be understood in terms of the mechanism described here.

We try to reproduce the geometrical structure of S 147 by assuming the existence of a few interstellar clouds in and around the shell. Table 2 gives the parameters which have been adopted by trial and error so that the result fits reasonably well the apparent orientations of filaments and a bright knot. We took the radius of S 147 to be 35 pc. Figure 13 illustrates the spatial distribution of the clouds in the coordinate system used in Table 2. Shaded clouds are those with low Alfven velocity, and unshaded ones with high Alfven velocity. Figure 14 shows the result, together with a photograph of this source for comparison. Some characteristic features are reproduced: a prominent long filament near the southern limb, which is an edge-on sheet filament due to an elongated low-V cloud No. 1; a bright knot in the EN quadrant as a result of focusing by the very low-V cloud No. 2; and large-scale deformations of the shell toward the east and west, which are caused by high-V clouds of larger scale (Nos. 3 and 4).

From Table 2 we see that the cloud diameter is required to be around 20 pc, which agrees satisfactorily with the typical diameter of the "standard" H I cloud (Spitzer, 1968). The above method of reproducing the observed features of filaments therefore provides information about such quantities as sizes, densities, magnetic fields and the three-dimensional distribution of the clouds. That is, the old supernova remnants can be used as interstellar probes on the basis of the present MHD method. Using the adopted values of Alfven velocities in Table 2, we have estimated field strengths at the centers of the clouds in S 147 for various assumed gas densities. Table 3 gives the result. Here we have assumed the intercloud values to be $n_0=0.05$ cm^{-3} and $B_0=4\,10^{-6}$ Gauss.

7. Discussion

i) Magnetic Fields

It is generally accepted that the interstellar magnetic fields are frozen in the gas because of the large electric conductivity. In the case of tangled magnetic lines of force the field strength varies with the gas density ρ as $B\propto\rho^{2/3}$, which means that the Alfven velocity depends on ρ as $V\propto\rho^{1/6}$. Hence, if the clouds are formed by contraction of interstellar gas with frozen-in magnetic fields, the clouds should have higher Alfven velocity than the intercloud region (Table 1). This situation will explain the existence of high-V clouds required for the reproduction of such features as protuberances, circular string filaments, and large-scale deformation of the SNR shell.

However, some clouds require lower Alfven velocity to reproduce the filaments and bright patches like those in S 147 in Figure 14. In fact, observations show that magnetic fields in dense interstellar clouds is of the order

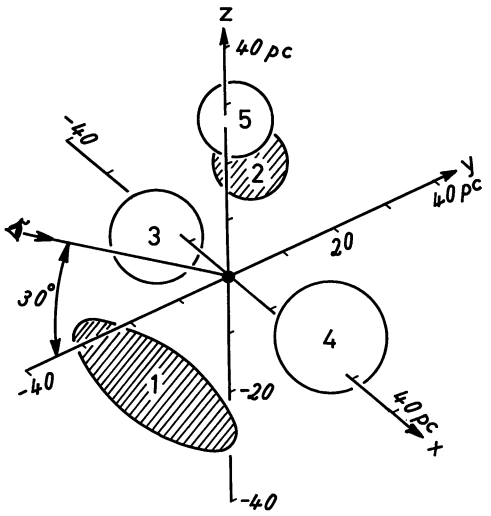

Fig. 13. Spatial distribution of interstellar clouds around the center of the supernova remnant, S 147. Shaded clouds have low Alfven velocities; unshaded clouds have high Alfven velocities. The coordinate system is chosen so that the line of sight is in the y-z plane and at 30° with the x-y plane. The SNR center is at the origin. See also Table 2

Table 3. Magnetic fields of the clouds in S 147 for some assumed gas densities

Cloud no.	$n=1$	10	100 cm^{-3}
1	$B=1.8\ 10^{-6}$	$5.6\ 10^{-6}$	$1.8\ 10^{-5}$ Gauss
2	$0.9\ 10^{-6}$	$2.8\ 10^{-6}$	$8.8\ 10^{-6}$
3	$3.6\ 10^{-5}$	$1.1\ 10^{-4}$	$3.6\ 10^{-4}$
4	$5.4\ 10^{-5}$	$1.7\ 10^{-4}$	$5.4\ 10^{-4}$
5	$2.8\ 10^{-5}$	$9.2\ 10^{-5}$	$2.8\ 10^{-4}$

Assumed intercloud values: $n_0=0.05$ cm^{-3}, $B_0=4\ 10^{-6}$ Gauss

of 10^{-5} Gauss, which yields $V\sim 10$ km s^{-1}, if the density is 10 cm^{-3}. This value of V is smaller than the velocity estimated on the premise that the fields are frozen-in (see Table 1). This fact suggests that the interstellar magnetic fields may not necessarily be frozen in the clouds. As the ambipolar process is too weak for the field to diffuse away from the cloud (Nakano, 1973), some unknown diffusion mechanism might work during the contraction of such low-V clouds.

In the above discussion, we have implicitly assumed that the clouds should have higher gas density than the intercloud space. However, as can be seen from Equation (8), our model depends only on the Alfven velocity. This means that the high-V cloud may possibly be replaced with a "hole" of gas having sufficient field strength. In fact, if a hole of gas exists with the density an order of magnitude more rarefied than the intercloud gas, or $\rho\sim 0.01$ cm^{-3}, and with the normal intercloud field, $B\sim 4\ 10^{-6}$ Gauss, then the Alfven velocity becomes three times as high as the surrounding region, or $V=3V_0(\varepsilon=2)$. In such a case of high-V hole, we must again abandon the hypothesis of frozen-in fields.

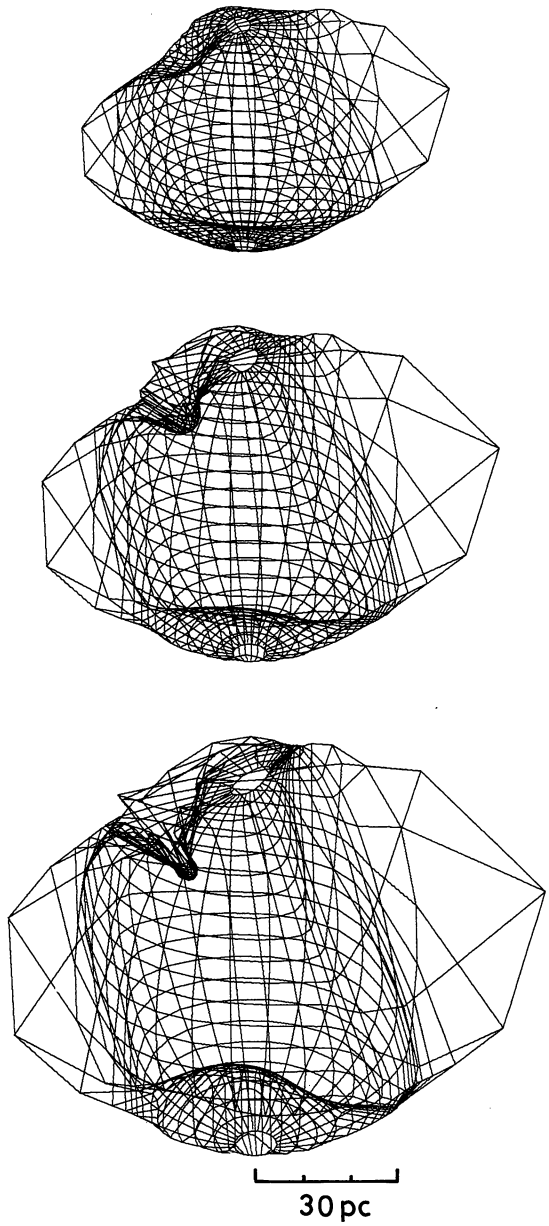

Fig. 14a. Simulation of the supernova remnant S 147 under the influence of several interstellar clouds, whose parameters are given in Table 2 and Figure 13. The second figure corresponds to the present S 147 whose photograph is shown in Figure 14b. Note a reproduction of some characteristic features as a filament near the southern limb, protuberances in the E and W sides, and a bright patch in the NE quadrant

ii) Effects of SNR *on a Dense Low-V Cloud*

As shown in Sections 3i) and 4ii), the MHD wave front strongly focuses on the central region of a cloud with a low Alfven velocity, which will result in a rapid increase of the amplitude growing into a strong shock wave, similar to a spherical implosion.

If the time scale of cooling of the gas τ_c, is shorter than the time taken for the skock to propagate through

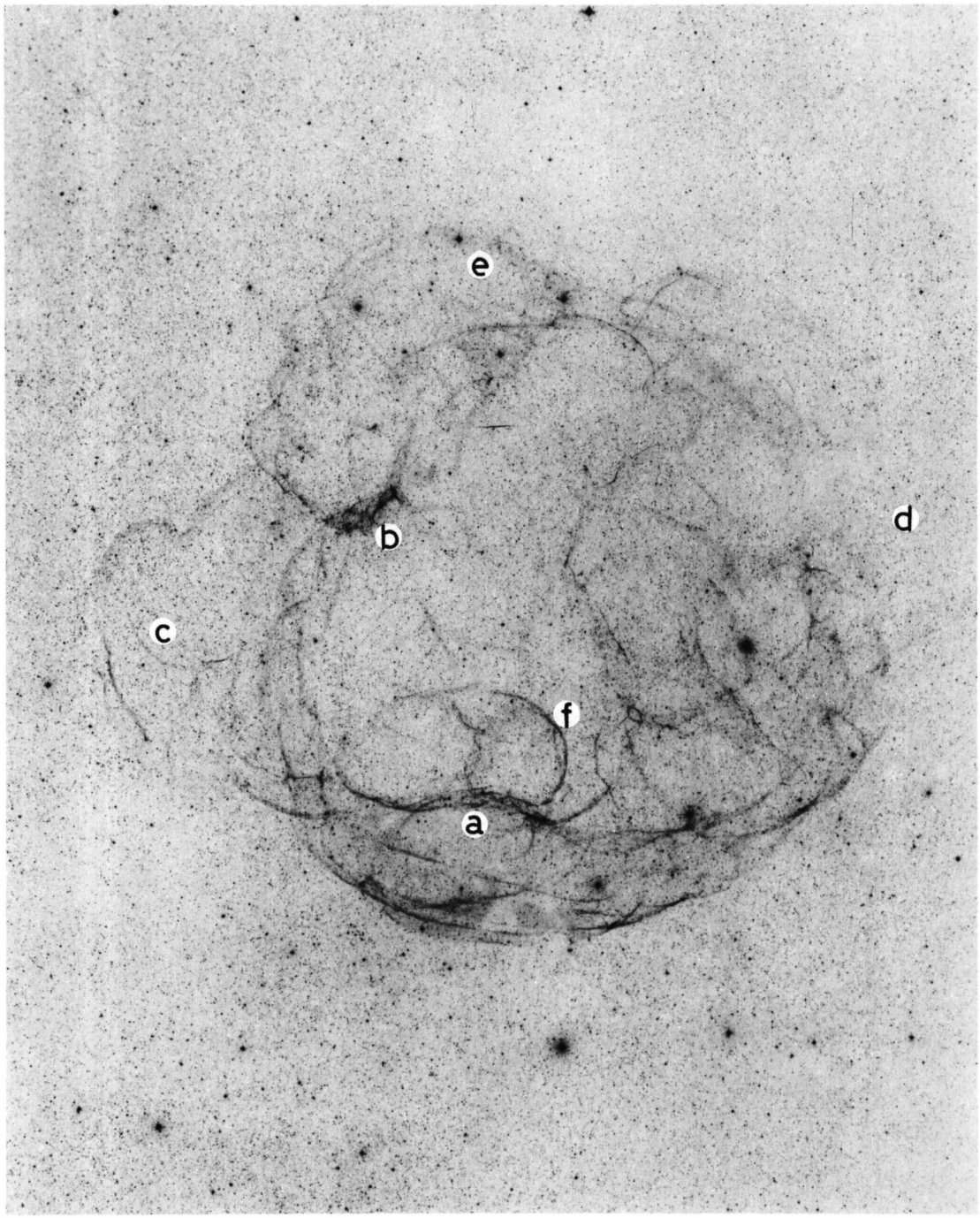

Fig. 14b. Supernova remnant S147, reproduced with permission from the SNR Atlas by van den Bergh et al. (1973) (Palomar Observatory photograph by van den Bergh). Compare with the second figure in Figure 14a. Some typical features are marked with *a–f* which are discussed in the text

the cloud, i.e. $\tau_c < r/V$ ($\sim 5\ 10^5$ yr if we take $r \sim 5$ pc and $V \sim 10$ km s^{-1}), a strong compression by the focusing shock will enhance thermal instability followed by a gravitational fragmentation of the cloud into small denser clouds. Further contraction of the fragments will evolve into sites of star formation. It is therefore possible that star formation will be enhanced in low-V interstellar clouds by the focusing of a SNR shock front even if the SNR is very old.

On the other hand, if $\tau_c > r/V$ and the dissipation of the shock is quick enough so that thermalization of the shock energy heats up a cloud increasing its internal pressure, the low-V cloud may be evaporated by a passage of the SNR shock front.

iii) Some Factors
Which Have Been Not Taken into Account

In the present paper, we have taken into account neither the effect of turbulent motion of the interstellar gas nor the internal motion of gas clouds. Such motions may not affect the evolution of SNRs in the present cases, because the expansion velocity of the shell considered here is much higher than both the turbulent and internal velocities of the clouds ($\sim 10\,\mathrm{km\,s^{-1}}$). This effect will become important when the shell radius exceeds, say, 50 pc. Before getting to this radius, however, any SNR would lose its identity and merge into the turbulent interstellar medium.

Another important factor which we have neglected is an initial anisotropy. As is well known, any SNR of early phase like the Crab Nebula has a more or less irregular morphology, and is not a simple sphere. This fact suggests that SNR expansion is already anisotropic in its initial phase. However, no theory has yet treated the development of an anisotropic explosion into a filamentary shell. Highly irregular filaments in young SNRs such as the Crab Nebula are probably due to magneto-hydrodynamic instabilities which are beyond the scope of this paper.

Acknowledgements. I wish to thank Prof. O. Hachenberg for the opportunity to stay at the MPIfR, and the Alexander von Humboldt-Stiftung for a Senior Research Fellowship. I thank also Dr. Y. Uchida of MPI für Physik und Astrophysik in München for valuable discussions, and Dr D. Downes of MPIfR for critical reading of the manuscript. The computations were carried out on the Cyber 172 of the MPIfR.

References

Assousa, G. E., Erkes, J. W.: 1973, *Astron. J.* **78**, 885
Chevalier, R. A.: 1974, *Astrophys. J.* **188**, 501
Chevalier, R. A., Gardner, J.: 1974, *Astrophys. J.* **192**, 457
Cox, D. P.: 1972a, *Astrophys. J.* **178**, 159
Cox, D. P.: 1972b, *Astrophys. J.* **178**, 169
Cornett, R. H.; Chin, G., Knapp, G. R.: 1977 (preprint)
Downes, D.: 1971, *Astron. J.* **76**, 305
Elliott, K. M., Gonick, C., Meaburn, J.: 1976, *Monthly Notices Roy. Astron. Soc.* **175**, 605
Heiles, C.: 1976, *Ann. Rev. Astron. Astrophys.* **14**, 1
Landau, L. D., Lifshitz, E. M.: 1960, Electrodynamics of Continuous Media, Pergamon Press, Oxford, Chap VIII
McKee, C. T., Cowie, L. L.: 1975, *Astrophys. J.* **195**, 715
Nakano, T.: 1973, *Publ. Astron. Soc. Japan* **25**, 91
Sgro, A.: 1975, *Astrophys. J.* **197**, 621
Sofue, Y.: 1976a, *Publ. Astron. Soc. Japan* **28**, 19
Sofue, Y.: 1976b, *Astron. Astrophys.* **48**, 1
Sofue, Y.: 1977, *Astron. Astrophys.* **60**, 327
Spitzer, L., Jr.: 1968, in *Stars and Stellar System VII;* Nebulae and Interstellar Matter, University of Chicago Press, eds. Middlehurst and Aller, Chapter I
Straka, W. C.: 1974, *Astrophys. J.* **190**, 59
Uchida, Y.: 1970, *Publ. Astron. Soc. Japan* **22**, 341
Uchida, Y.: 1974, *Solar Phys.* **39**, 431
Uchida, Y.; Altschuler, M. D., Newkirk, H. Jr.: 1973, *Solar Phys.* **28**, 495
van den Bergh, S.; Marscher, A. P., Terzian, Y.: 1973, *Astrophys. J. Suppl.* **26**, 19
Woltjer, L.: 1972, *Ann. Rev. Astron. Astrophys.* **10**, 129